Thin Solid Films 660 (2018) 242–246

Contents lists available at ScienceDirect

Thin Solid Films

journal homepage: www.elsevier.com/locate/tsf

Synthesis of nanocrystalline δ-MoN by thermal annealing of amorphous thin films grown on (100) Si by reactive sputtering at room temperature

N. Haberkorn[a,b,*], S. Bengio[a], H. Troiani[a,b], S. Suárez[a,b], P.D. Pérez[a], M. Sirena[a,b], J. Guimpel[a,b]

[a] Centro Atómico Bariloche, Comision Nacional de Energía Atómica, Consejo Nacional de Investigaciones Científicas y Técnicas, Av. Bustillo 9500, 8400 San Carlos de Bariloche, Argentina

[b] Instituto Balseiro, Universidad Nacional de Cuyo, Comision Nacional de Energía Atómica, Av. Bustillo 9500, 8400 San Carlos de Bariloche, Argentina

ARTICLE INFO

Keywords:
Metal Nitrides
Sputtering
Superconductivity

ABSTRACT

We report on the synthesis and characterization of nanocrystalline δ-MoN by crystallization of amorphous thin films grown on (100) Si by reactive sputtering at room temperature. Films with chemical composition MoN were grown using a deposition pressure of 5mTorr with a reactive mixture of $Ar/(Ar + N_2) = 0.5$. The as-grown films display mostly amorphous structure. Nanocrystalline δ-MoN phase is obtained after annealing at temperatures above 600 °C. The superconducting critical temperature T_c depends on film thickness. Thick films (170 nm) annealed at 700 °C for 30 min display a $T_c = 11.2$ K (close to the one reported for bulk specimens: 13 K), which is gradually suppressed to 7.2 K for 40 nm thick δ-MoN films. Our results provide a simple method to synthesize superconducting nitride thin films on silicon wafers with T_c above the ones observed for conventional superconductors such as Nb.

1. Introduction

The synthesis of superconducting transition-metal nitrides is of technological relevance in the design of devices such as tunnel junctions [1] and electromagnetic radiation detectors [2, 3]. The molybdenum nitrides present several superconducting crystalline phases: γ-Mo_2N (cubic) with $T_c \sim 5$ K [4], β-Mo_2N (tetragonal) with superconducting critical temperature $T_c \sim 5$ K [5] and δ-MoN (hexagonal) with $T_c \sim 13$ K [6, 7]. Thin films of the different crystalline structures have been sintered through chemical and physical routes [8–13]. An outstanding feature for γ-Mo_2N and δ-MoN is that sharp superconducting transitions have been observed for epitaxial and polycrystalline thin films [14–16]. Moreover, superconductivity has been observed for films with thicknesses of a few nanometers [14, 15, 17]. Recently, we have reported that the chemical concentration and T_c for Mo-N thin films grown at room temperature by reactive sputtering can be modified by changing the Ar:N_2 ratio [18]. Films grown with $N_2/(Ar + N_2) < 0.4$ mixtures are superconducting with nanocrystalline γ-Mo_2N phase. Films grown with $N_2/(Ar + N_2) > 0.4$ mixtures are mostly amorphous with a stoichiometry Mo/N ≈1 (close to the one corresponding to δ-MoN). These amorphous films do not display superconducting transition. It is worth noting that the δ-MoN phase displays T_c higher than Nb (hence, displays larger superconducting gap $\Delta = 1.76 * k_B * T_c$). In addition, hexagonal δ–MoN is the hardest superconductor metal nitride (relevant for coating) [7].

In this work, we report the synthesis of nanocrystalline δ-MoN by crystallization of amorphous thin films. Initially, stoichiometric MoN thin films are grown by reactive DC sputtering at room temperature on AlN buffered (100) Si substrates using a $N_2/(Ar + N_2) = 0.5$ mixture. As-grown thin films display a residual-resistivity ratio $RRR = R^{300K}/R^{onset} \approx 0.8$. Nanocrystalline δ-MoN phase with $RRR > 1$ is obtained after annealing at temperatures above 600 °C. The annealed films display very smooth surfaces. The superconducting critical temperature T_c is strongly affected by the film thickness. The successful synthesis of δ-MoN thin films on Si substrates by a controllable and reproducible route (with low roughness values), enhances the potential applications in superconducting devices.

2. Material and methods

MoN films were deposited on 8 nm thick AlN buffered Si (100) substrates by reactive DC magnetron sputtering using a $N_2/(Ar + N_2) = 0.5$ mixture without any intentional heating of the substrate [17, 18]. The AlN buffer layer was introduced to avoid any chemical reaction between the Mo and the SiO_2 cup layer of the Si wafers. AlN was selected because it displays high stability at interfaces with transition metal nitrides [1]. However, no appreciable differences in T_c were observed for thin films grown with and without the buffer

* Corresponding author.
E-mail address: nhaberk@cab.cnea.gov.ar (N. Haberkorn).

https://doi.org/10.1016/j.tsf.2018.06.010
Received 26 December 2017; Received in revised form 1 April 2018; Accepted 6 June 2018
Available online 07 June 2018

layer (not shown). The residual pressure of the chamber was < 10^{-6} Torr. Ultra-high purity Ar (99.999%) and N_2 (99.999%) were used as gas sources. The AlN and MoN layers were grown by RF (100 W) and DC (50 W) magnetron sputtering, respectively. During deposition the target to substrate distance was ~5.5 cm. The total pressure at the chamber was 5 mTorr. AlN buffer layers were grown using a N_2/(Ar + N_2) = 0.2 mixture [17]. The deposition rate for MoN using a N_2/(Ar + N_2) = 0.5 mixture was ≈17 nm/min. Thermal annealing was performed in vacuum (to avoid surface contamination) with a residual pressure of 10^{-5} Torr at temperatures between 400 °C and 700 °C during periods of 30 min. In order to homogenize the temperature, the films were enveloped in a tantalum foil during the annealing procedure. Wherever used, the notation [*d*-T] corresponds to samples with thickness *d* annealed at *T* °C (with *T* = 400 °C, 600 °C and 700 °C) for 30 min. The results shown here correspond to 40 nm, 60 nm, 100 nm and 170 nm thick MoN films. However, most studies are performed in 170 nm thick MoN films, which display the highest T_c.

X-ray diffraction (XRD) patterns were obtained with a Panalytical Empirean equipment. The structure was studied by transmission electron microscopy (TEM) with a Philips CM200UT microscope operating at 200 kV. The TEM specimen was prepared by scraping the surface of a film with a diamond tip. The topology of the films was characterized by atomic force microscopy (AFM) measurements in a Dimension 3100©Brucker microscope. The AFM images were obtained in tapping mode. The chemical composition and thickness of the films were analyzed by Rutherford Backscattering Spectroscopy (RBS) with a TANDEM accelerator using a 2 MeV $4He^{2+}$ ion beam. Surface composition analysis was performed by X-ray photoelectron spectroscopy (XPS) using a standard Al/Mg twin-anode X-ray gun and a hemispherical electrostatic electron energy analyzer (high vacuum conditions with a base pressure of 10^{-9} Torr). The electrical transport measurements were performed using the standard four-point configuration. Magnetization measurements were performed in a SQUID magnetometer. Critical current densities (J_c) were estimated considering the Bean model [19].

3. Results and discussion

The chemical composition of the films was verified using RBS. The composition $MoN_{(1.00 \pm 0.05)}$ was observed for pristine and annealed specimens. As-grown MoN thin films using a N_2/(Ar + N_2) = 0.5 mixture are mostly amorphous (a little reflection attributed to γ Mo_2N is observed) [18]. The crystallization of δ-MoN after thermal annealing at temperatures above 600 °C was confirmed by XRD (see Fig. 1). The lattice parameters calculated from the (002) and (200) diffraction peaks, are *a* = 0.572(2) nm and *c* = 0.555(3) nm. These values are close to those observed in epitaxial δ-MoN [12]. Fig. 2*a*, *b*, *c* show TEM images for [170–700]. Fig. 2*a* shows a cross section bright field TEM image where the film thickness homogeneity can be observed. Fig. 2*b* shows a dark field image obtained from the $(200)_{\delta\text{-MoN}}$ ring (see selected area electron diffraction (SAED) in the inset). The bright regions in the image correspond to nanometric δ-MoN grains with typical size between 5 nm and 10 nm. In addition, the 201 reflection -corresponding to a superficial MoO_3 layer- is observed in the SAED [17]. Fig. 2*c* shows a high resolution TEM image of δ-MoN grains. The spots corresponding to the 200 reflections are identified for one of the grains. In addition, planes at distances of ≈0.248 nm can be identified from Fourier filtered image. Fig. 3*a* shows the AFM image for [170–700] (smother surfaces are observed for thinner films). The film displays a very smooth surface, only a few small morphologic inhomogeneities with a height < 6 nm are observed (see profile in Fig. 3*b*). The Root Mean Square (RMS) roughness for an area of 5 μm^2 is 0.6 nm, which indicates that (compared to as-grown films) crystallization does not significantly alter the morphology of the films [17]. The weak influence of the annealing in the surface topology can be attributed to the crystallization of grains with diameter of a few nanometers.

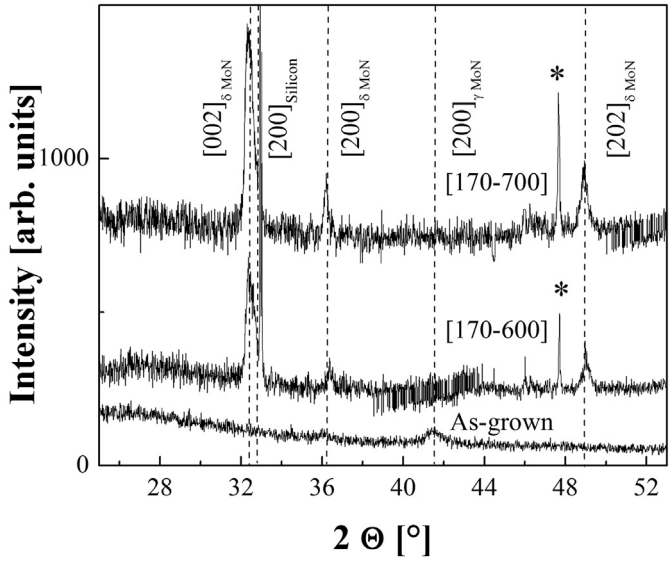

Fig. 1. X-ray diffraction pattern for a 170 nm thick MoN thin film: as grown and annealed (600 °C and 700 °C). (*) Silicon reflections.

XPS measurements were performed to obtain information about the chemical composition of the film and the chemical state of the Mo. The photoelectron peaks Mo3d, O1s, C1s and N1 s were measured in detail. An overlap of the N1 s and the Mo3p peaks was observed. In order to remove components related to superficial C and MoO_3, the surface of the films was cleaned with Ar^+ sputtering (2 kV) [17]. The Mo3d binding energy region for the surface of as-grown films and [170–700] thin films is shown in Fig. 4*a* and *b*, respectively. The thickness of the MoO_3 surface layer was estimated in 1.6 nm using the XPS Mo3d intensities of the MoO_3 and MoN phase [20]. In the as-grown Mo3d spectra two components were identified: a major component at BE = 228.9 eV attributed to the δ-MoN phase, and a minor component at BE = 228.5 eV attributed to the γ-Mo_2N phase [21, 22]. In the [170–700] films only one major component was identified at BE = 228.9 eV, which can be assigned to the δ-MoN phase. Besides, in both spectra there is an extra component at higher binding energies that can be ascribed to different causes: unscreened peaks of the present phases as observed for MoO_2 [23], the presence of Mo^{4+} associated to MoO_2 impurities or as a consequence of overlooking possible asymmetric behavior of the main components, as suggested for MoO_2 [24].

The dependence of T_c with the thickness for annealed films was analyzed measuring the electrical resistance as function of the temperature. To understand the influence of the thermal annealing on the electrical properties, initially a 170 nm thick MoN film was annealed at different temperatures (see Fig. 5*a*). As-grown thin films display a *RRR* ≈0.8 (indicative of high disorder with very short electronic mean free path *l*). After crystallization to δ-MoN (at ≈600 °C), the films show a metallic behavior. For [170–600] and [170–700], the *RRR* values are ≈1.3 and ≈1.5, and they display a superconducting transition with T_c = 10.5 K and 11.2 K, respectively (see inset Fig. 5*a*). The superconducting transition width (defined as in Fig. 5*b*) is ≈1 K for [170–600] and ≈0.6 K [170–700]. A common feature for films with different thickness is that for longer annealing periods (> 30 min) or for higher annealing temperatures (> 700 °C), neither T_c is increased nor the superconducting transition width is reduced. In particular, annealing temperatures higher than 800 °C produce cracks on the surface, which is evidenced in wider superconducting transitions without percolation. Fig. 5*b* shows the superconducting transition observed for films with different thickness after annealing at 700 °C. The results show that T_c is gradually suppressed by thickness even for films as thicker as 100 nm (T_c = 10.7 K). For epitaxial δ-MoN thin films, the reduction in T_c is usually observed for films thinner than 40 nm [27]. In

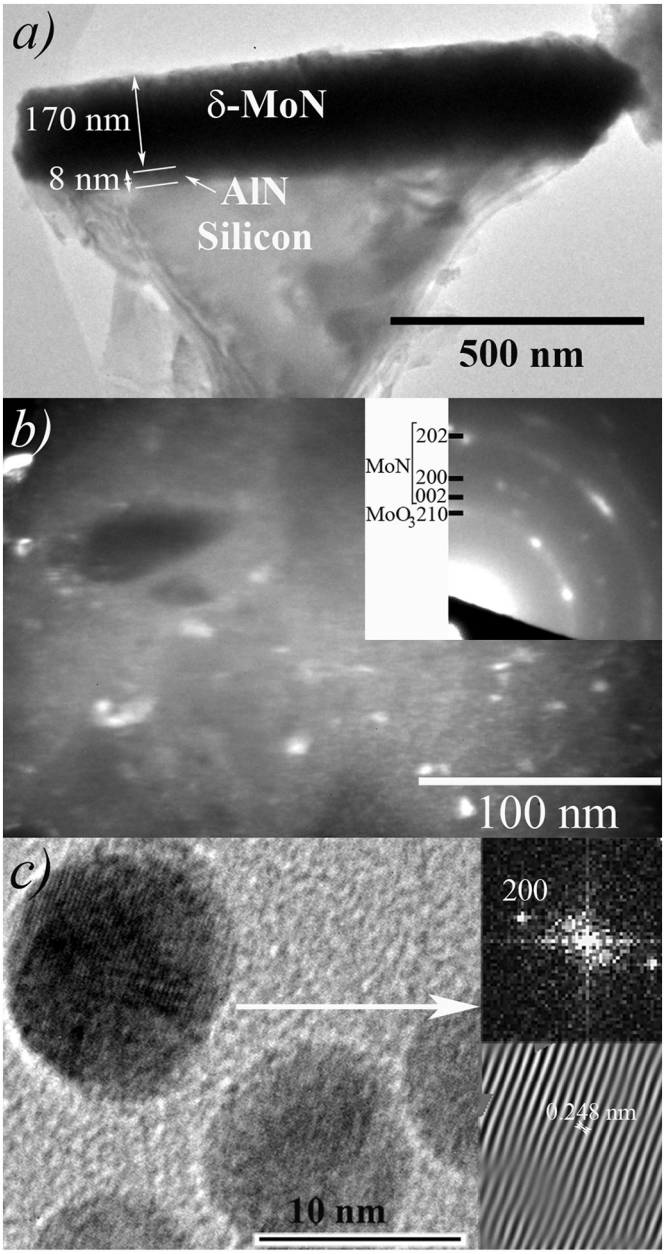

Fig. 2. TEM images for a 170 nm thick δ-MoN film ([700]). *a*) Bright field cross section TEM image. *b*) Dark field plan view image using the $(002)_{\delta\text{-MoN}}$. Inset shows the corresponding SAED pattern. *c*) High resolution TEM image of nanograins. The fast Fourier transformation and the filtered image obtained using the 200 spots for one of the grains are included.

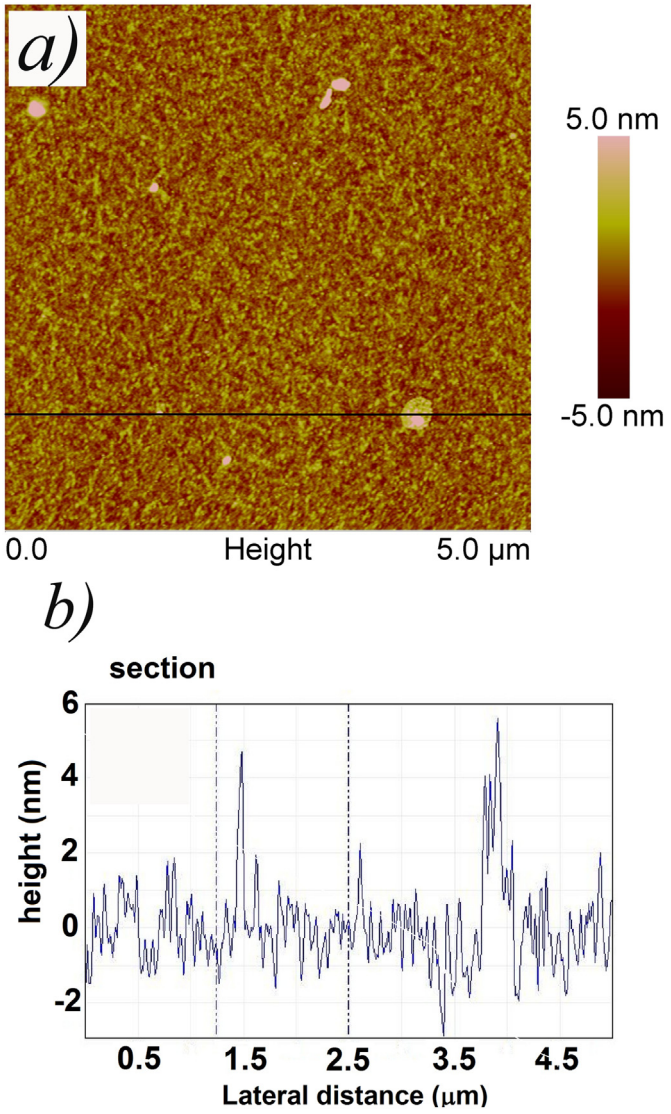

Fig. 3. *a*) 5 × 5 μm^2 topographical AFM of a 170 nm thick MoN film after being annealed at 700 °C. *b*) AFM profile for the line indicated in *a*).

our case, T_c for $d = 40$ nm decreases to 7.2 K, indicating that the thickness affects the crystallization. The results obtained for [170–600] and [170–700] suggest that the thickness dependence of T_c may be related to changes in the disorder and in the average grain size. Detailed studies of the microstructure are necessary to clarify this point.

Following we analyzed the temperature dependence of the upper critical field H_{c2} (T) for [170–600] and [170–700], which allows to analyze the influence of T_c on H_{c2} (T) for the 3 dimensional (3D) limit ($d >>$ coherence length ξ). Fig. 6 shows H_{c2} (T) for the [170–600] and [170–700] with the magnetic field perpendicular ($H_{c2}^{\perp}$) and parallel ($H_{c2}^{\parallel}$) to the surface. Inset in Fig. 6 shows comparison between H_{c2} and the irreversibility line H_{irr} (related to the superconducting transition width ΔT). The results show negligible upper critical field anisotropy ($\gamma = H_{c2}^{\perp}/H_{c2}^{\parallel} \approx 1$), which is in agreement with the expectations for 3D polycrystalline thin films. The temperature dependence of $H_{c2}^{\perp}$ can be analyzed by the WHH model developed for dirty one-band superconductors [25], which is given by:

$$ln\frac{1}{t} = \sum_{v=-\infty}^{\infty}\left(\frac{1}{|2v+1|} - \left[|2v+1| + \frac{\hbar}{t} + \frac{(\alpha\hbar/t)^2}{|2v+1| + (\hbar + \lambda_{so})/t}\right]^{-1}\right) \quad (1)$$

where $t = T/T_c$, $\hbar = (4/\pi^2)(H_{c2}(T)/|dH_{c2}/dT|_{T_c})$, α is the Maki parameter which quantifies the weakening influence of the Pauli electron spin paramagnetism on the superconducting state, and λ_{so} is the spin-orbit scattering constant. The WHH formula - satisfies the relation

$$H_{c2}(0) = \frac{H_{c2}^{orb}(0)}{\sqrt{1+\alpha^2}} \quad (2)$$

when $\lambda_{so} = 0$ [26]. The H_{c2} (T) curves can be adjusted considering $\alpha = 0$, $\lambda_{so} = 0$ and $-|dH_{c2}/dT|_{T_c} \approx 1$ T/K (see dotted lines in Fig. 6). The parameter $\alpha = 0$ corresponds to a pure "orbital field limit" due to supercurrents circulating around the vortex cores. The $H_{c2}(0)$ obtained from the extrapolation to zero field of the WHH model are 7.5 T (ξ (0) = 6.6 nm) and 7.8 T (ξ (0) = 6.5 nm) for [170–600] and [170–700], respectively. These values are lower than the ≈10 T previously

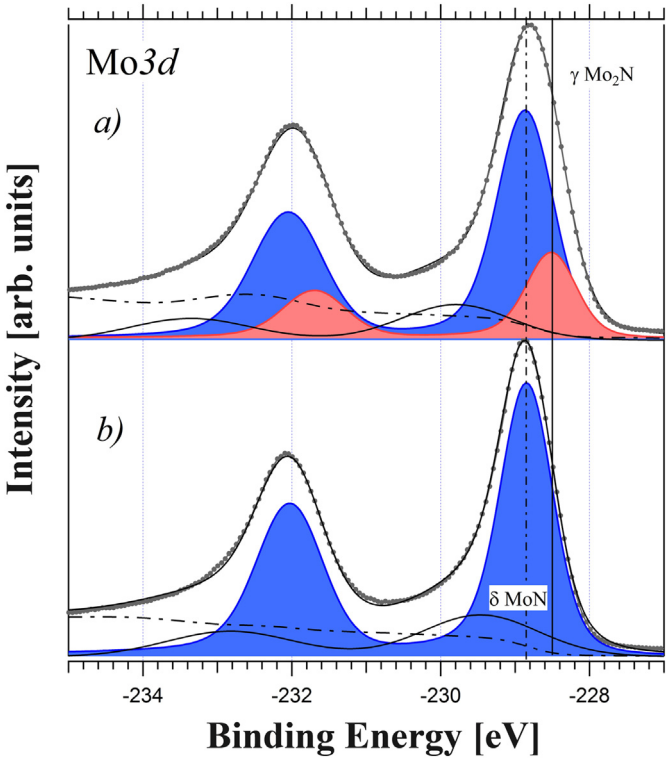

Fig. 4. XPS Mo3d spectra of: *a*) As-grown MoN thin films. *b*) MoN film after being annealed at 700 °C ([170–700]).

obtained in epitaxial and dirty δ-MoN sintered for polymer assisted deposition [27]. From very basic considerations $\xi_0 \propto \nu_F/T_c$, where ν_F is the Fermi velocity [28]. Similar $\xi_0 T_c$ values (≈70 nm*K) are obtained for [170–600] and [170–700] and the films reported in Ref. [27] ($\xi_0 T_c = 5.6\,\text{nm} * 12.6\,\text{K}$), which indicates that the reduction in $H_{c2}(0)$ can be mainly attributed to the suppression of T_c (corresponding to films in the dirty limit with very short electronic mean free path *l*).

Finally, for comparison with δ-MoN obtained by chemical methods [12, 15], the J_c (*H*) dependences at 4.5 K for [100–700] and [170–700] were obtained (see Fig. 7). At low fields both samples display thermal vortex jumps, which affect the magnetization (see inset Fig. 7). The J_c (*H*) dependences are plotted for $\mu_0 H > 0.05$ T. The obtained values J_c at low fields are $\approx 1.24\,\text{MA cm}^{-2}$[100–700] and $\approx 1.8\,\text{MA cm}^{-2}$ [170–700], which are comparable to those reported for epitaxial thin films in refs. [12, 15] (with values above 1 MA cm^{-2} for $T = 4.5$ K).

4. Conclusions

In summary, we report on the synthesis and the superconducting properties in nanocrystalline δ-MoN thin films. Initially, amorphous MoN thin films were grown by reactive sputtering at room temperature on Si wafers. In a second step, the films were crystallized in vacuum to avoid surface contamination, at temperatures between 600 °C and 700 °C. The annealed films display very smooth surfaces (relevant for tunnel junctions) and a polycrystalline microstructure with nanometric grain size. The superconducting critical temperature T_c is strongly affected by the film thickness. Films thicker than 100 nm display $T_c > 10$ K, being 11.2 K for $d = 170$ nm. The reported simple process to synthesize δ-MoN thin films with adequate physical properties on Si substrates enhances its potential for developing different technological applications, varying from radiation sensors to Josephson tunnel junctions.

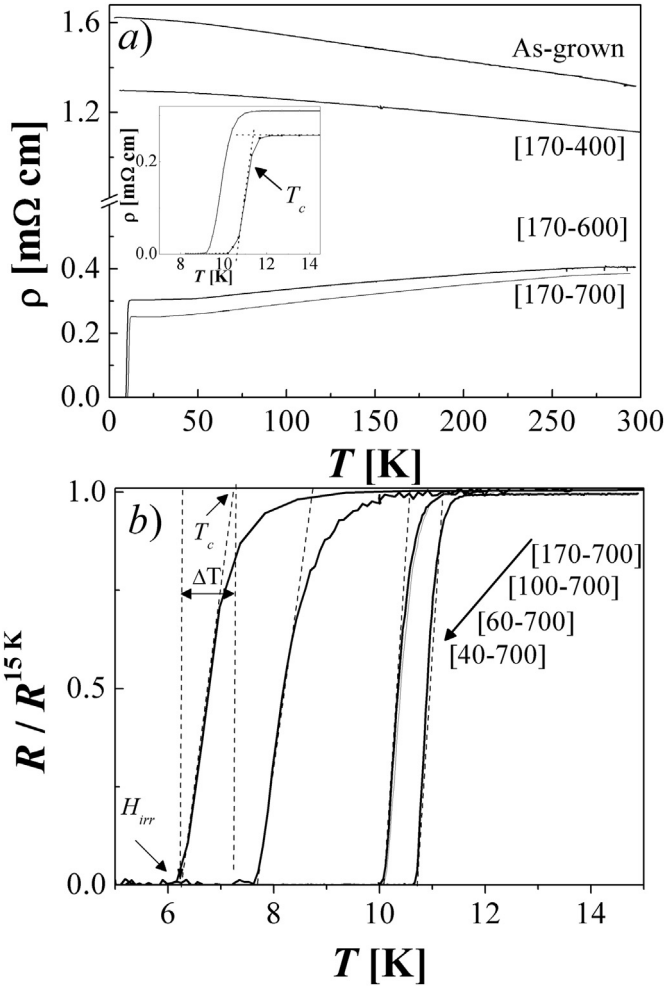

Fig. 5. *a*) Temperature dependence of the resistance for an as-grown thin film, [170–400], [170–600] and [170–700]. Inset shows the temperature dependence of [170–600] and [170–700] at temperatures smaller than 20 K and the criteria for the determination of T_c. *b*) Temperature dependence of the normalized resistance for [40–700], [60–700], [100–700] and [170–700].

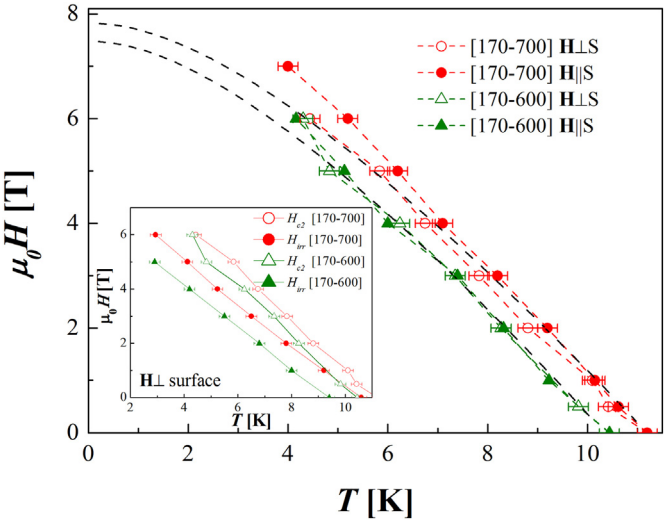

Fig. 6. Temperature dependence of the upper critical field (H_{c2}) and irreversibility line (H_{iee}) with **H** parallel and perpendicular to the surface for [170–600] and [170–700]. Inset shows a comparison between H_{c2} and the irreversibility line H_{irr} for [170–600] and [170–700] (related to the superconducting transition width).

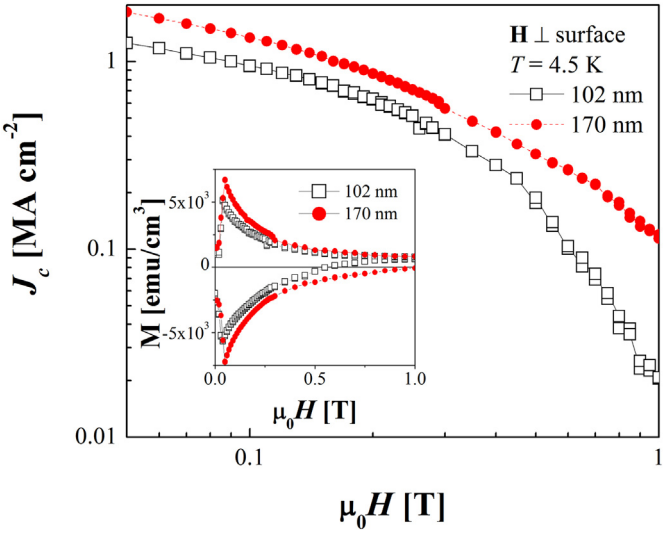

Fig. 7. Log-log plots of critical current density (J_c) versus applied magnetic field (H) of [100–700] and [170–700] at 4.5 K. Inset shows isothermal **M** versus **H** curves at 4.5 K applying different magnetic field **H** perpendicular to the surface.

Acknowledgments

We thank C. Olivares for technical assistance. This work was partially supported by the ANPCyT (PICT 2015-2171), Universidad Nacional de Cuyo06/C505 and CONICETPIP 2015-0100575CO. NH, SB, MS and JG are members of the Instituto de Nanociencia y Nanotecnología, CNEA-CONICET.

References

[1] Zhen Wang, Hirotaka Terai, Akira Kawakami, Yoshinori Uzawa, Interface and tunneling barrier heights of NbN/AlN/NbN tunnel junctions, Appl. Phys. Lett. 75 (1999) 701–703.
[2] M. Shcherbatenko, I. Tretyakov, Yu. Lobanov, S.N. Maslennikov, N. Kaurova, M. Finkel, B. Voronov, G. Goltsman, T.M. Klapwijk, Nonequilibrium interpretation of DC properties of NbN superconducting hot electron bolometers, Appl. Phys. Lett. 109 (2016) 132602–132605.
[3] Chandra M. Natarajan, Michael G. Tanner, Robert H. Hadfield, Superconducting nanowire single-photon detectors: physics and applications, Supercond. Sci. Technol. 25 (2012) 063001.
[4] B.T. Matthias, J.K. Hulm, A search for new superconducting compounds, Phys. Rev. 87 (1952) 799–806.
[5] Kei Inumaru, Kazuya Baba, Shoji Yamanaka, Synthesis and characterization of superconducting β-Mo_2N crystalline phase on a Si substrate: an application of pulsed laser deposition to nitride chemistry, Chem. Mater. 17 (2005) 5935–5940.
[6] Kei Inumaru, Takanori Nishikawa, Kazuharu Nakamura, Shoji Yamanaka, High-pressure synthesis of superconducting molybdenum nitride δ-MoN by in situ nitridation, Chem. Mater. 20 (2008) 4756–4761.
[7] Shanmin Wang, Daniel Antonio, Xiaohui Yu, Jianzhong Zhang, Andrew L. Cornelius, Duanwei He, Yusheng Zhao, The hardest superconducting metal nitride, Sci. Rep. 5 (2015) 13733.
[8] Y.H. Shi, B.R. Zhao, Y.Y. Zhao, L. Li, J.R. Liu, Superconducting and normal-state properties of MoN_x thin films, Phys. Rev. B 38 (1988) 4488–4491.
[9] H. Ihara, M. Hirabayashi, K. Senzaki, Y. Kimura, H. Kezuka, Superconductivity of B1-MoN films annealed under high pressure, Phys. Rev. B 32 (1985) 1816–1817.
[10] Kei Inumaru, Kazuya Baba, Shoji Yamanaka, Structural distortion and suppression of superconductivity in stoichiometric B1-MoN epitaxial thin films, Phys. Rev. B 73 (2006) 52504.
[11] D.K. Christen, S.T. Sekula, J.T. Ellis, J.D. Lewis, J.M. Williams, Formation, properties, and ion irradiation effects of hexagonal structure MoN thin films, IEEE Trans. Magn. 23 (1987) 1014–1018.
[12] Y.Y. Zhang, et al., Epitaxial superconducting δ-MoN films grown by a chemical solution method, J. Am. Chem. Soc. 133 (2011) 20735–20737.
[13] Hongmei Luo, Guifu Zou, Haiyan Wang, Joon Hwan Lee, Yuan Lin, Huisheng Peng, Qianglu Lin, Shuguang Deng, Eve Bauer, T. Mark, Anthony K. McCleskey, QuanxiJia Burrell, Controlling crystal structure and oxidation state in molybdenum nitrides through epitaxial stabilization, J. Phys. Chem. C 115 (2011) 17880–17883.
[14] Takuya Tsuneoka, Kazumasa Makise, Sho Maeda, Bunju Shinozaki, Fusao Ichikawa, Localization and pair breaking parameter in superconducting molybdenum nitride thin films, J. Phys. Condens. Matter 29 (2017) 015701.
[15] Hanlu Zhang, et al., Self-assembled *c*-axis oriented δ-MoN thin films on Si substrates by chemical solution deposition: growth, transport and superconducting, J. Alloys Compd. 704 (2017) 453–458.
[16] R. Baskaran, A.V. Thanikai Arasu, E.P. Amaladass, L.S. Vaidhyanathan, D.K. Baisnab, Increased upper critical field for nanocrystalline MoN thin films deposited on AlN buffered substrates at ambient temperature, J. Phys. D 49 (2016) 205304–205307.
[17] N. Haberkorn, S. Bengio, H. Troiani, S. Suárez, P.D. Pérez, P. Granell, F. Golmar, M. Sirena, J. Guimpel, Thickness dependence of the superconducting properties of γ-Mo_2N thin films on Si (001) grown by DC sputtering at room temperature, Mater. Chem. Phys. 204 (2018) 48–57.
[18] N. Haberkorn, S. Bengio, S. Suárez, P.D. Pérez, M. Sirena, J. Guimpel, Effect of the nitrogen-argon gas mixtures on the superconductivity properties of reactively sputtered molybdenum nitride thin films, Mater. Lett. 215 (2018) 15–18.
[19] a C.P. Bean, Magnetization of hard superconductors, Phys. Rev. Lett. 8 (1962) 250–253;
b Magnetization of High-Field Superconductors, Rev. Mod. Phys. 36 (1964) 31–39.
[20] M.R. Alexander, G.E. Thompson, X. Zhou, G. Beamson, N. Fairley, Quantification of oxide film thickness at the surface of aluminium using XPS, Surf. Interface Anal. 34 (2002) 485–489.
[21] Kejun Zhang, Lixue Zhang, Xiao Chen, Xiang He, Xiaogang Wang, Shanmu Dong, Lin Gu, Zhihong Liu, Changshui Huang, Guanglei Cui, Molybdenum nitride/N-doped carbon Nanospheres for lithium-O_2 battery cathode electrocatalyst, Appl. Mater. Interfaces 5 (2013) 3677–3682.
[22] Z.B. Zhaobin Wei, P. Grange, B. Delmon, XPS and XRD studies of fresh and sulfided Mo_2N, Appl. Surf. Sci. 135 (1998) 107–114.
[23] David O. Scanlon, Graeme W. Watson, D.J. Payne, G.R. Atkinson, R.G. Egdell, D.S.L. Law, Theoretical and experimental study of the electronic structures of MoO_3 and MoO_2, J. Phys. Chem. C 114 (2010) 4636–4645.
[24] J. Baltrusaitis, B. Mendoza-Sanchez, V. Fernandez, R. Veenstra, N. Dukstiene, A. Robert, N. Fairley, Generalized molybdenum oxide surface chemical state XPS determination via informed amorphous sample model, Appl. Surf. Sci. 326 (2015) 151–161.
[25] N.R. Werthamer, E. Helfand, P.C. Hohenberg, Temperature and purity dependence of the superconducting critical field, Hc2. III. Electron spin and spin-orbit effects, Phys. Rev. 147 (1966) 295–302.
[26] K. Maki, Effect of pauli paramagnetism on magnetic properties of high-field superconductors, Phys. Rev. 148 (1966) 362–369.
[27] N. Haberkorn, Y.Y. Zhang, J. Kim, T.M. McCleskey, A.K. Burrell, R.F. Depaula, T. Tajima, Q.X. Jia, L. Civale, Upper critical magnetic field and vortex-free state in very thin epitaxial d-MoN films grown by polymer-assisted deposition, Supercond. Sci. Technol. 26 (2013) 105023.
[28] M. Tinkham, Introduction to Superconductivity, 2 edition, Dover Publications, New York, 2004.